Journal of Applied Fluid Mechanics, Vol. 16, No. 10, pp. 1927-1937, 2023.
Available online at www.jafmonline.net, ISSN 1735-3572, EISSN 1735-3645.
https://doi.org/10.47176/jafm.16.10.1759

Effect of Blade Twist on The Flow Characteristics of Gas-Liquid Two-Phase Flow in a Spiral Axial Flow Pump

W. Han[1], H. Feng[1†], Z. Xu[1], Y. Hao[1], J. Zhang[1] and C. Yang[1,2]

[1] *College of Energy and Power Engineering, Lanzhou University of technology, Lanzhou, Gansu province 730050, China*
[2] *James Watt Schllo of Engineering, The University of Glasgow, Glasgow G12 8QQ, UK*

†*Corresponding Author Email: fhmm0117@163.com*

ABSTRACT

The mixing of oil and gas forms the foundation of deep-sea oil and gas extraction and transportation. However, traditional conveying equipment has low efficiency and high failure rates. In this study, a spiral axial flow gas and liquid multiphase pump was used as the base model. The Eulerian multiphase flow model and RNG turbulence model were used for numerical simulations to analyze the internal flow field of the multiphase pump. A modification scheme was proposed to twist the airfoil shape and create a twisted vane. The twisted blade with the center of the hub-side flange chord length as the twisting center was twisted in the counterclockwise direction to help reduce the relative volume of gas in the flow channel. When the twisted vane with the hub-side airfoil type trailing edge point as the twisting center was twisted in the suction side direction, it helped to accelerate the movement of the gas-liquid mixture at the trailing edge of the back of the vane and further reduced the low velocity zone at the back of the vane. When the twist center is located at the hub side wing type trailing edge point of the twist vane, the twist degree is 0.214. This results in the maximum head and efficiency of the pump, improves gas phase aggregation phenomenon, and enhances the performance of the multiphase pump.

Article History

Received January 15, 2023
Revised May 8, 2023
Accepted May 24, 2023
Available online July 29, 2023

Keywords:

Spiral axial flow pump
Gas-liquid two-phase flow
Blade twist
Internal flow characteristics
Gas-phase aggregation

1. INTRODUCTION

The components of deep-sea oil resources are extremely complex and generally include numerous impurities, gases, and other liquids. It is difficult to use traditional ordinary pumps in deep-sea locations for the stable and effective transport of oil resources because they can easily experience clogging and other problems, which can cause serious damage to the entire oil pipeline.

Therefore, in order to reduce the wear and tear of an oil pipelines and extend their service life, the development of a new multiphase pump is particularly important (Di et al. 2012). In the axial vane mechanical classification, an axial multiphase pump considers the dual performance of both a compressor and a liquid-phase pump. Li & Xue (2000) referred to several existing studies to effectively replace the oil and gas separation equipment required in the original oil and gas mixed transfer equipment. This simplifies the transfer structure, improves the transfer efficiency, and reduce the costs. Some studies have shown that changing the degree of twist of the vanes can improve the performance of rotating machinery. Lumsdaine & Cherng (1976) found that twisted and non-twisted vanes, vane thickness, and other factors had a significant impact on the external characteristics of axial flow compressors. They also determined that an appropriate angle for the twisted vane shape could effectively enhance the hydraulic performance of axial flow compressors. Kumar & Saini (2017) found that turbines with twisted blades perform better at lower flow rates. The twisted blades were simulated and optimized using a CFD analysis technique. The numerical analysis was based on the non-constant Reynolds mean equation solver with the k-ε turbulence model. The maximum power coefficient was obtained at twist angles of 12.5–23°. Zhu et al. (2012) implemented a twisted design for the blade section of a cross-flow fan and conducted numerical simulations for both straight and twisted blades. The two types of fans were compared experimentally, and it was found that the performance of the twisted-blade cross-flow fan was better than that of the straight-blade cross-flow fan at a twisting angle of 60°. This provides new ideas for the design and selection of cross-flow fan blades. Zhang & Feng (2015) adapted the traditional straight-blade turbine by transforming it into a twisted-blade turbine, and conducted numerical simulations and tests on the two types of turbines. They found that the

NOMENCLATURE

τ	degree of twist	ρ_k	densityt
f_k	mass force	R_{vog}	Relative volume of gas
M_k	surface tension	Ψ	Head coefficient
P	Pressure	η	efficiency
U_k	Fluid velocity in the compression unit stage	H	Head
μ_{eff}	effective viscosity factor		

twisted blade could improve the hydraulic efficiency of the turbine as well as a provide better hydraulic performance under the same working conditions. When studying the pressure pulsation characteristics of centrifugal pumps, Shi et al. (2018) found that changing the twist angle of the original vanes could improve the external characteristics of centrifugal pumps, enhance the flow state of the fluid in the flow channel, and make the internal flow field more uniform and stable. Deng et al. (2014) studied the effects of twisted and cylindrical vanes on the external characteristics of centrifugal pumps. They found that the pressure at the inlet of the cylindrical-vane centrifugal pumps was more susceptible to the effects of shaft frequency. Lv et al. (2012) found that the external characteristics of straight-blade and twisted-blade vertical-axis wind turbines differed significantly. The authors concluded that the performance of the twisted-blade wind turbines was better than that of the straight-blade wind turbines. Liu (2005) programmed a forward-curved blade, reverse-curved blade, and swept-back blade and used the FLUENT fluid calculation software to conduct a three-dimensional numerical calculation of the internal flow field of a pump with various blades. By comparing and analyzing the gas volume and efficiency inside the pump with different blades, it was found that the backward-curved blade exhibited the best anti-cavitation performance.

Although many studies have investigated the effect of blade twist on the mechanical performance, they have mainly focused on wind turbines, while few have studied the effect of blade twist on the performance of gas–liquid multiphase pumps. During the transportation of a mutiphase pump, gas–liquid separation leads to an accumulation of air bubbles, thus blocking the flow channel and decreasing the performance of the mutiphase pump. In this study, we propose a modification scheme based on the twisting of an airfoil to form a twisted vane and conduct numerical simulations to compare the external and internal flow characteristics of the modified scheme with those of the original scheme. This allows us to obtain a scheme that effectively reduces the degree of gas-phase aggregation in the flow channel of the mutiphase pump and prevent or improve the gas-phase aggregation in the flow channel.

2. SPIRAL AXIAL FLOW MULTIPHASE PUMP NUMERICAL CALCULATION METHOD

2.1 Three-dimensional Modeling of the Spiral Axial-Flow Multiphase Pump

In this study, a spiral axial impeller with a specific speed of n_s=214.4 was used as the power component, and its design flow rate Q_0=100 m^3/h, head H=30 m, and speed n=4500 rpm.

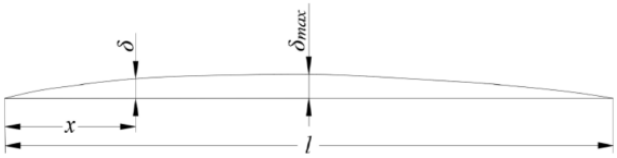

Fig. 1 Blade airfoils for impellers and guide vanes

Table 1 791 Wing type thickening law

x/l	0	0.05	0.075	0.1	0.2	0.3	0.4
δ/δ_{max}	0	0.296	0.405	0.489	0.778	0.92	0.978
x/l	0.5	0.6	0.7	0.8	0.9	0.95	0.1
δ/δ_{max}	1	0.88	0.756	0.544	0.356	0.2	0

2.1.1 Wing Type Selection

In this study, the thickness variation law of the 791 wing type was chosen to thicken the vanes of the multiphase pumps, as shown in Fig. 1. The vane thickening law is shown in Table 1. where x is the length from the leading edge of the airfoil, l is the chord length of the airfoil, δ represents the thickness at position x, and δmax is the maximum thickness of the airfoil.

2.1.2 Design of the Compression Unit

The airfoil parameters are listed in Table 2. They were located near the hub at the airfoil for face5 and near the wheel rim at the airfoil for face1, as shown in Fig. 2. Five airfoil cross sections were defined for face1 to face5. An impeller blade was installed using five airfoil cross sections for surface mixing. The working surface and the back surface of the blade were then formed.

The impeller and guide vanes are the compression units of the multiphase pump. The main geometric dimensions are listed in Table 3 and shown in Fig. 3, while the calculation domain is displayed in Fig. 4.

Table 2 Impeller section surface airfoil parameters

Wing position	Cross-sectional diameter d(m)	String length L(m)	Maximum thickness δ_{max}
face1	0.15	0.236	0.005
face2	0.14	0.22	0.006
face3	0.13	0.204	0.007
face4	0.12	0.188	0.008
face5	0.11	0.172	0.009

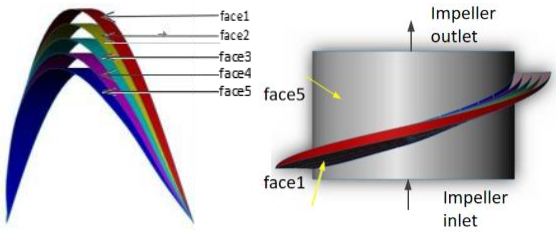

Fig. 2 3D schematic diagram of different airfoil

Table 3 Main dimensional parameters of the impeller and guide vane inside the multiphase pump

Impeller design main parameters		Main parameters of guide lobe design	
Rim diameter Dt_1	150mm	Rim diameter Dt_2	150mm
Impeller hub inlet diameter dh_1	110mm	Diameter of guide lobe hub inlet dh_3	122mm
Impeller hub outlet diameter dh_2	122mm	Outlet diameter of guide lobe hub dh_4	110mm
Number of blades Z	4	Number of blades Z	17
Blade axial length e	55mm	Axial length of guide vane	55mm
Wheel half-taper angle γ	6°	Wheel half-taper angle γ	6°
Blade inlet placement angle β_1	10°	Blade inlet placement angleβ_3	38°
Blade exit placement angle β_2	14°	Blade exit placement angleβ_4	90
		Axial distance between guide vane and impeller	8

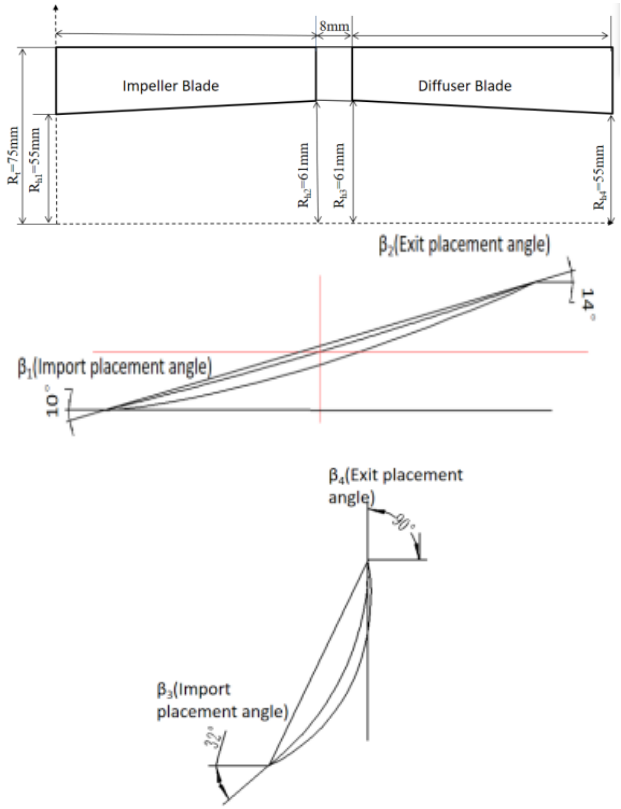

Fig. 3 Impeller guide vane hydraulic design diagram

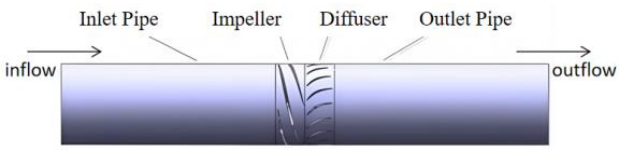

Fig. 4 Three domains of overflow components

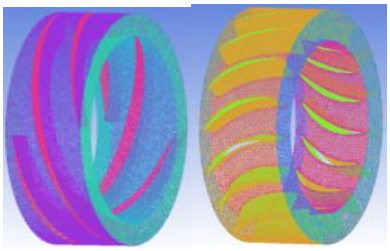

(a) Impeller (b) Guide vane

Fig. 5 Schematic diagram of impeller and guide vane grid

2.2 Numerical Simulation Basis of Spiral Axial Flow Mutiphase Pump

2.2.1 Grid Division

In this study, ANSYS ICEM17.0 was used to mesh the water body diagrams of each overflow component of the spiral axial-flow pump. Because the impeller and guide vane of the spiral axial-flow pump contain surfaces with large curvature changes, it was difficult to use structured meshes for classification. To facilitate the encryption of local areas, the inlet extension, impeller, guide vane, and outlet extension of the spiral axial-flow pump were divided using unstructured meshes. In the division of the mesh, the maximum size was 1.5 mm because the blade pressure surface and suction surface are the main parts of the study; thus, there is a need for this part of the mesh division to be encrypted (encryption size of 1 mm). Figure 5 shows the grids of the impeller and guide vane.

2.2.2 Mesh Irrelevance Test

To improve the accuracy of calculation results and reduce the waste of computational resources, it was necessary to conduct a grid irrelevance check for the entire basin of the mutiphase pump to determine the best grid division method. In this study, Eqs (1) and (3) were used to calculate the head and efficiency of different grid numbers. Figure 6 shows the mesh irrelevance test for the entire basin of the mutiphase pump with 50% gas content at the inlet. After analysis, a final mesh number of 7,161,420 was obtained.

The formula for the head is

$$H = \frac{\Delta P}{\rho_m g} \tag{1}$$

where the differential pressure between the import and export $\Delta P = P_2 - P_1$

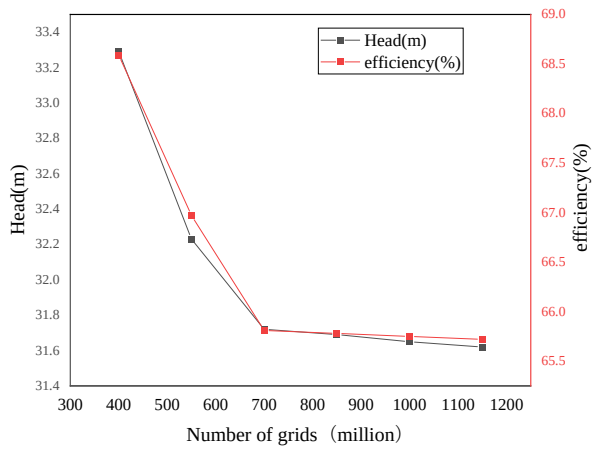

Fig. 6 Mesh irrelevance test for the entire mutiphase pump

The density of the mixed medium is:

$$\rho_m = \alpha_g \rho_g + \alpha_l \rho_l \tag{2}$$

The formula for efficiency is:

$$\eta = \frac{\rho_m g Q H}{M\omega} \tag{3}$$

2.3 Numerical Calculation Methods

2.3.1 Gas-liquid Two-phase Flow Theory

Gas–liquid two-phase flow was studied by assuming an incompressible continuous medium. Other assumptions were that there was no temperature exchange between the two phases, no generation of phase change, and no energy exchange, to satisfy the continuous-medium theory.

In the continuity equation, the fluid microcluster mass increase per unit time is equal to the net mass flow rate into the fluid microclusters.

$$\frac{\partial}{\partial t}(\alpha_k \rho_k) + \nabla \cdot (\alpha_k \rho_k U_k) = 0 \tag{4}$$

Where k denotes the phase (gas phase-*g*; liquid phase-*l*; solid phase, s), α_k denotes the volume fraction, U_k denotes the fluid velocity at the compression unit stage (m/s), and ρ_k denotes the density (kg/m^3).

In the momentum equation, the sum of the various external forces acting on the microfluid is equal to the rate of change in the momentum of the microfluid with respect to time.

where k denotes the phase (gas phase-*g*; liquid phase-*l*), p denotes the pressure (Pa), f_k denotes the mass force (N), and M_k denotes the surface tension (N).

2.3.2 Turbulence Model

Turbulence phenomena are widespread in nature, and their mobility is extremely complex. The RNG κ-ε turbulence model is a modified equation based on the standard κ-ε model. It takes into account the rotation in the mean flow and the vortex phenomenon during flow. It also adds the term Rε to the ε equation, which reflects the mainstream time-averaged strain rate, thereby increasing the accuracy of numerical simulations, making it suitable for high strain rates and flow lines with large curvatures. For flow, the RNG κ-ε turbulence model was selected using the following control equations. Further information is available in Zhang & Feng (2005).

The κ equation is:

$$\frac{\partial}{\partial t}(\rho k) + \frac{\partial}{\partial x_i}(\rho u_i k) = \frac{\partial}{\partial x_j}\left[\partial_k \mu_{eff} \frac{\partial k}{\partial x_j}\right] + G_k + \rho\varepsilon \tag{6}$$

The ε equation is:

$$\frac{\partial}{\partial t}(\rho\varepsilon) + \frac{\partial}{\partial x_i}(\rho u_i \varepsilon) = \frac{\partial}{\partial x_j}\left[\alpha_\varepsilon \mu_{eff} \frac{\partial \varepsilon}{\partial x_j}\right] + \frac{C_{1\varepsilon}^* \varepsilon}{k} G_k - G_{2\varepsilon}\rho \frac{\varepsilon^2}{k} \tag{7}$$

$C_{1\varepsilon}$=1.42, $C_{2\varepsilon}$=1.68, C_μ=0.085, α_k =1.39, α_ε=1.39; G_k denotes the generation of turbulent kinetic energy due to the mean velocity gradient; G_b denotes the turbulent kinetic energy generated by buoyancy; Y_M denotes the contribution of fluctuating expansion to the total dissipation rate in compressible turbulent flows; σ_k and σ_ε are the turbulent Prandtl numbers of *k* and *ε*, respectively; and μ_{eff} is the effective viscosity factor, and is calculated as:

$$\mu_{\text{eff}} = \mu + \mu_t \tag{8}$$

μ denotes the molecular viscosity coefficient; μ_t denotes the turbulent viscosity coefficient.

In this study, FLUENT 17.0 was used for numerical simulation. The Eulerian model was chosen with water as the main phase and air in the form of bubbles as the second phase. The fluid was assumed to be incompressible for constant calculations. The turbulence model was adopted as an RNG κ-ε turbulence model. The velocity–pressure coupling calculation was adopted as the phase-coupled SIMPLE algorithm. The inlet boundary condition was a velocity inlet of 3.4 m/s. The volume of the second phase was set as the inlet gas volume fraction (IGVF). The inlet gas–water mixture was set as a homogeneous mixture. The pressure outlet was set as the outlet boundary condition. Reference values were selected from the system's default pressure values. A no-slip solid wall condition was used as the flow boundary condition, and the standard wall function method was used to solve the fluid flow near the wall. The inlet, guide vane, and outlet domains were selected from a static coordinate system. The impeller domain was selected from the dynamic coordinate system. The convergence residual was set to 0.00001.

$$\frac{\partial}{\partial t}(\alpha_k \rho_k U_k) + \nabla \cdot (\alpha_k \rho_k U_k U_k - \alpha_k \tau_k) = -\alpha_k \nabla p + M_k + \alpha_k \rho_k f_k \tag{5}$$

3. EFFECT OF TWISTED VANES BASED ON AIRFOIL TORSION ON THE PERFORMANCE OF MUTIPHASE PUMPS

The blade structure of the spiral axial-flow gas-liquid multiphase pump impeller determines the transport performance of the pump. Optimizing the blade structure of the mutiphase pump can effectively improve gas-liquid

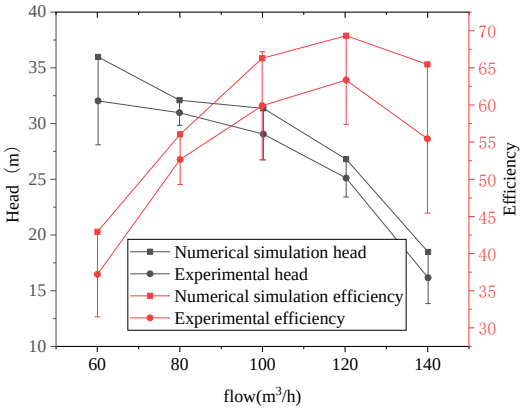

(a) IGVF=30%

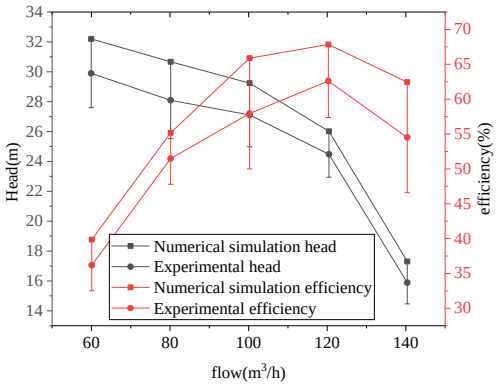

(b) IGVF=50%

Fig. 7 Comparison between numerical simulation and experimental external characteristics of mutiphase pump

separation and aggregation. While optimizing the vane structure can prevent significant separation of the mixed liquid in the flow channel, it is also essential to consider the mutiphase pump's pressurization performance to avoid phase separation. Therefore, it is crucial to ensure that both phases are uniformly mixed to prevent laminar flow or gas aggregation.

3.1 Numerical Method Validation of Spiral Axial Flow Mutiphase Pump

Based on the gas–liquid two-phase flow test bench, the external characteristics of the multiphase pump were tested at n=4500 rpm; IGVF of 30% and 50%; and flow rates of $0.6Q_0$=60 m^3/h, $0.8Q_0$=80 m^3/h, Q_0=100 m^3/h, $1.2Q_0$=120 m^3/h, and $1.4Q_0$=140 m^3/h for the five flow conditions, respectively. The external characteristics of the mutiphase pump were tested and compared with the results of a numerical simulation of the external characteristics under the same conditions, as shown in Fig. 7.

As shown in Fig.7, the numerical simulation results were consistent with the experimental results. At an inlet gas content of 30% and a design flow rate (Q_0) of 100 m^3/h, the numerical simulation showed a head (H) and efficiency (η) of 31.4 m and 66.2%, respectively, for the mutiphase pump. The test results for the same conditions showed a head (H) and efficiency (η) of 29.2 m and 60%, respectively. At an inlet gas content of 50% and a design flow rate (Q_0) of 100 m^3/h, the numerical simulation showed a head (H) and efficiency (η) of 29.32 m and 65.96%, respectively, for themutiphase pump. The test results for the same conditions showed a head (H) and efficiency (η) of 27.12 m and 57.89%, respectively. The error between the numerical simulation and experimental results of the mixed transfer pump, with varying inlet gas contents, was within 10% at the design flow point. This range is reasonable due to the loss of gas-liquid two-phase flow during actual operation. Additionally, the numerical simulation results for the external characteristics of the multiphase pump were consistent with the experimental results, indicating the reliability and accuracy of the chosen calculation method for the numerical simulation.

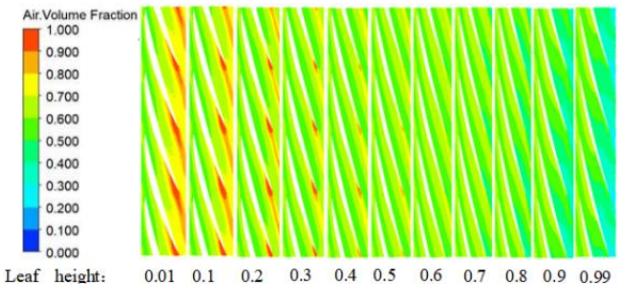

Fig. 8 Gas volume fraction at different leaf heights of the original model

3.2 Numerical Simulation of Spiral Axial Flow Multiphase pump

After performing the numerical simulation of the original model at a rated speed of 4,500 rpm and a rated flow rate of 100 m^3/h with a 60% gas content at the inlet, the gas volume fraction clouds at different leaf heights in the impeller domain were extracted.

As shown in Fig. 8, the gas volume fraction gradually increased along the wheel edge towards the hub side in the impeller runner of the mixed pump. The gas-phase aggregation phenomenon became more evident as the gas volume fraction in the middle of the runner approached the IGVF. The gas-phase aggregation area was mainly concentrated on the hub side at the back of the blade near the outlet, where the gas volume fraction increased and the gas aggregated. The separation of gas bubbles in the flow channel was primarily due to the pressure gradient force and centrifugal force, which caused an imbalance. To alleviate the gas-liquid separation phenomenon in the impeller, the blade's original model structure was modified at a low leaf height (leaf height of 0.1 to 0.3). This improved the gas-phase aggregation phenomenon without requiring a redesign of the entire impeller blade. Only the position of the face5 wing section near the hub changed, while the other wing sections remained the same. This led to the formation of a twisted vane in the multiphase pump numerical model, which was analyzed for its external and internal flow characteristics under different modification schemes. This allowed for the exploration of the best twisting law required for optimal performance of the multiphase pump.

3.3 Blade Reformulation Scheme

This study proposes three twisted vanes that are based on airfoil twists. Scheme 1 is based on the rotation center of the leading-edge point of the face5 airfoil, Scheme 2 is based on the rotation center of the chord length center of

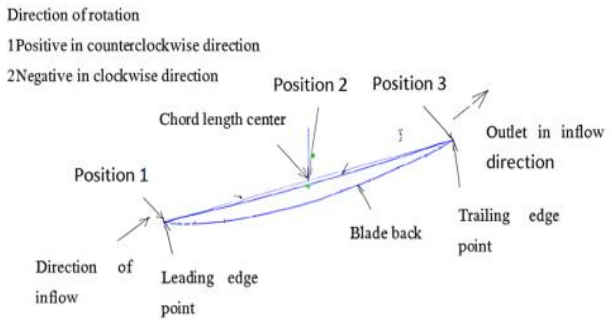

Fig. 9 Schematic diagram of airfoil rotation

the face5 airfoil, and Scheme 3 is based on the rotation center of the trailing-edge point of the face5 airfoil. A schematic diagram of the reshaping process is shown in Fig. 9.

3.3.1 Twisting Based on Face5 Airfoil Leading-edge Point as The Center of Rotation

This study demonstrates that the torsion angle causes the impeller blade face4 to exhibit a twisted structure. The face5 airfoil section was rotated with different rotation centers and then wrapped and twisted on its corresponding circumferential surface, where the angle of twist was $\Delta\theta$. The face5 airfoil section had three rotational center positions, with counterclockwise rotation considered positive and clockwise rotation considered negative. The degree of twist was introduced to express the degree of twisting of face4, with a placement angle of 14° for the face4 wing section serving as the reference. The degree of twist, τ, of the face4 surface was defined as follows:

$$\tau = \frac{\Delta\theta}{14^{\circ}} \tag{9}$$

Where τ_1 represents the degree of distortion of face4 when wing section face5 is rotated around the leading edge point as the center of rotation, τ_2 represents the degree of distortion of face4 when wing section face5 is rotated around the center of the chord length of the airfoil as the center of rotation, τ_3 denotes the degree of distortion of face4 when wing section face5 is rotated around the trailing edge point of the airfoil as the center of rotation, and |τ| denotes the magnitude of the twist value.

The degree of twist indicates the magnitude of the torsion angle of the face5 airfoil section at each torsion center. At the same time, it also indicates the degree of twisting of the face4. As there are two directions of the twist angle, τ is indicated using positive and negative signs. A negative sign indicates twisting in the clockwise direction, and a positive sign indicates twisting in the counterclockwise direction. The twisting parameters are listed in Table 4.

As shown in Fig. 10, only the face 5 airfoil section was modified to rotate around the leading edge point of the airfoil as the center of rotation. The face5 airfoil section was then wrapped around its corresponding circumferential surface. The leading edge point of the airfoil was used as the center of twist on its wrapped circumferential surface, where $-0.214 < \tau_1 < +0.214$. As illustrated in the schematic diagram in Fig. 11, the other

Table 4 Torsion parameters based on the leading edge point of the airfoil as the center of rotation

Wing position	Rotation Center	Torsion degree
face5 airfoil	Leading edge point	$\tau_1 = -0.214$
		$\tau_1 = -0.142$
		$\tau_1 = -0.0714$
		$\tau_1 = 0.0714$
		$\tau_1 = 0.142$
		$\tau_1 = 0.214$

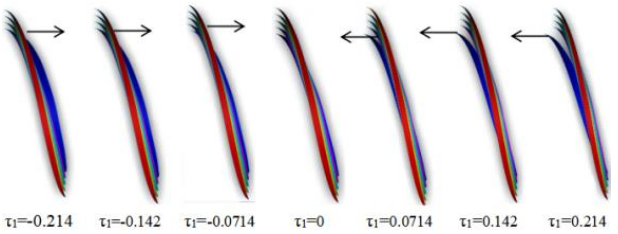

Fig. 10 Schematic diagram after twisting based on the leading edge point of the airfoil as the center of rotation (the arrows denote the direction of rotation)

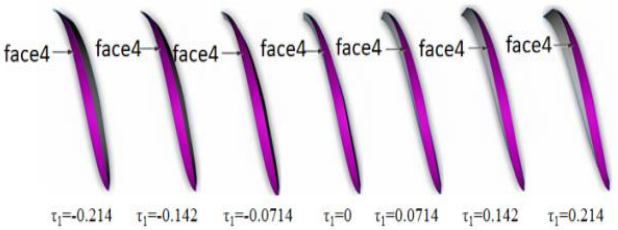

Fig. 11 Schematic diagram of face4 after wing twist

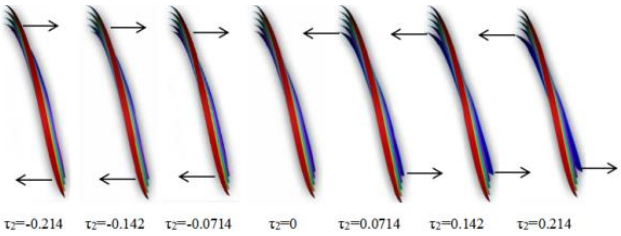

Fig. 12 Schematic diagram after twisting based on the center of chord length of the airfoil as the center of rotation (the arrows denote the direction of rotation)

corresponding airfoil sections did not undergo any twisting or translation after the face5 airfoil was twisted. When the face5 airfoil section was twisted in the clockwise direction, Blade S4 shifted towards the suction side. The closer it was to the trailing edge of the blade, the greater the shift towards the suction side. When the airfoil's face5 section was twisted in the counterclockwise direction, blade s4 shifted towards the pressure side. The more it shifted towards the pressure side, the further it moved towards the trailing edge of face4.

3.3.2 Twisting Based on the Chord Length Center of the Face5 Airfoil as the Center of Rotation

Figure 12 shows that only the airfoil section face5 was changed to rotate around the chord length center as the

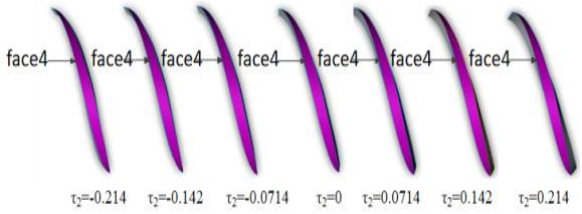

Fig. 13 Schematic diagram of face4 after wing twist

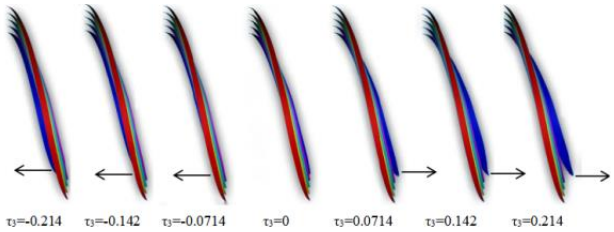

Fig. 14 Schematic diagram after twisting based on the wing trailing edge point as the center of rotation (the arrows denote the direction of rotation)

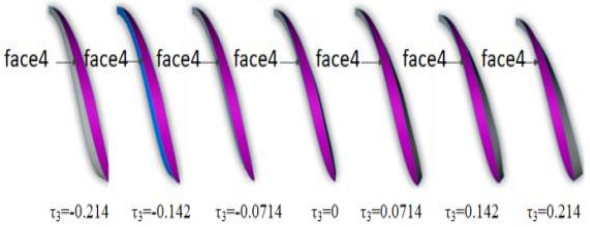

Fig. 15 Schematic diagram of face4 after wing twist

center of rotation, and the section was wrapped around its corresponding circumferential surface. The chord length center was used as the center of twist on its wrapped circumferential surface, where $-0.214 < \tau_2 < +0.214$. Figure 13 depicts a schematic diagram of the position of the twisted airfoil face5 in relation to the other airfoil sections. The other airfoils remained neither torsional nor translational. When the airfoil section face5 was twisted clockwise, the blade leading edge face4 shifted towards the pressure side, and the trailing edge of the blade shifted towards the suction side. When the airfoil section face5 was twisted counterclockwise, the blade leading edge face4 shifted towards the suction side, and the trailing edge shifted towards the pressure side.

3.3.3 Twisting Based on Face5 Airfoil Trailing Edge Point as The Center of Rotation

As shown in Fig. 14, only the airfoil section face5 was modified to rotate around the trailing-edge point, and then wrapped around its corresponding circumferential surface. The face5 section was twisted on its wrapped circumferential surface with the trailing-edge point of the airfoil as the center of the twist, where $-0.214 < \tau_3 < +0.214$. Figure 15 displays a schematic diagram of the position of airfoil face5 after twisting, relative to the other airfoil sections. The other airfoils were not twisted or translated. When airfoil section face5 was twisted clockwise, blade face4 shifted toward the pressure side, with a stronger shift closer to the blade head. When airfoil section face5 was twisted counterclockwise, blade face4 shifted toward the suction side, with a stronger shift closer to the blade leading edge.

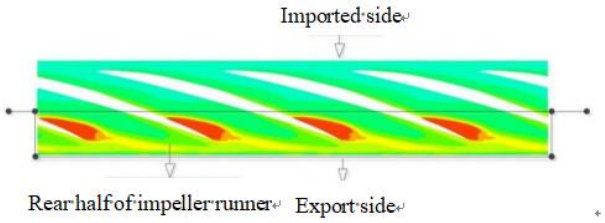

Fig 16. Schematic diagram of the analysis area (grid area size is 0.009810810827m^2)

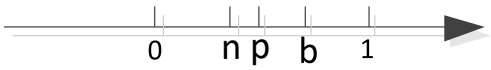

Fig. 17 Bell curve of gas phase distribution

3.4 Relative Volume of Gas and Head Coefficient

The main area of gas-phase aggregation was the low-blade-height area. Therefore, relevant data was used to extract the volume fraction of the gas phase at 0.1 of the blade height, and the corresponding grid area size. The area of gas-phase aggregation at a low blade height was mainly in the rear half of the impeller. As shown in Fig. 16, an area of 0.1 of the blade height was selected as the object of analysis.

The relative volume of gas (R_{vog}) is a coefficient that indicates the degree of gas retention and aggregation.

$$R_{vog} = \frac{S_{vof>b}}{S_{vof>p}} \tag{10}$$

Assuming that the inlet gas content is n, it is known from the gas-phase distribution diagram that the average value of the gas volume fraction in the second half of the impeller was p, as shown in Fig. 17.

Moreover, because of the aggregation effect, the value of p was greater than that of n. Similarly, the normal curve was bell-shaped, with low ends and a high center, and was symmetrical along the vertical axis. In the second half of the impeller, the gas-phase distribution showed a trend similar to a normal distribution, with the middle value of p indicating that the grid area occupied by the gas-water mixture with a gas volume fraction of p in the second half of the impeller was the largest, and the two ends were lower. This indicates that separation and aggregation of the gas and liquid phases occurred in the second half of the impeller. The low position on the left side indicates the separation of a large number of gas phases and a decrease in the gas volume fraction, whereas the right side indicates a large amount of gas aggregation and an increase in the gas volume fraction. The b value corresponds to the larger value on the right side of a similar normal distribution. The gas-water mixture with a volume fraction greater than the b value is considered to represent the large amount of gas-phase stagnation and aggregation phenomena occurring in this zone. The b value needs to be satisfied.

$$\frac{1-b}{1-p}=0.5 \tag{11}$$

R_{vog} can be considered as the relative degree of gas-phase aggregation in the second half of the impeller in a mutiphase pump. This concept is applicable to impeller sections with different inlet gas content. R_{vog} indicates the ratio of the gas-water mixture with a large volume fraction of the gas phase in the second half of the impeller to the overall flow path, as well as the size of the area of large gas-phase accumulation in the second half of the impeller to the overall area of the upper flow path.

Head coefficient Ψ:

$$\Psi=\frac{H}{u_2^2/2g} \tag{12}$$

where, u_2 is the impeller inlet circumferential velocity; H is the head; and g is the gravitational acceleration.

3.5 Effect of Twisted Vanes Based on Airfoil Twist on the External Characteristics and Relative Volume of the Gas of the Multiphase Pump

Schemes 1, 2, and 3 were chosen to analyze the R_{vog}, head, and efficiency for a 50% inlet gas content.

As shown in Fig. 18, in the comparison of the three modification schemes, Scheme 3 had a better modification effect than the other two schemes. The modification in Scheme 3 had the largest and best effect on R_{vog}, with R_{vog} being reduced to 0.13 at the lowest point in Scheme 3. The gas-phase aggregation area of the flow channel was smaller, resulting in a more stable flow. When comparing the same τ case, the R_{vog} of Scheme 3 was smaller than that of the other two schemes.

To study the variations in the external characteristic parameters of the multiphase pump in the scheme, the variation law between the degree of twist of the multiphase pump and the external characteristic performance parameters was revealed. This was achieved by establishing the mathematical equations for the degree of twist and the R_{vog}, head coefficient, and efficiency.

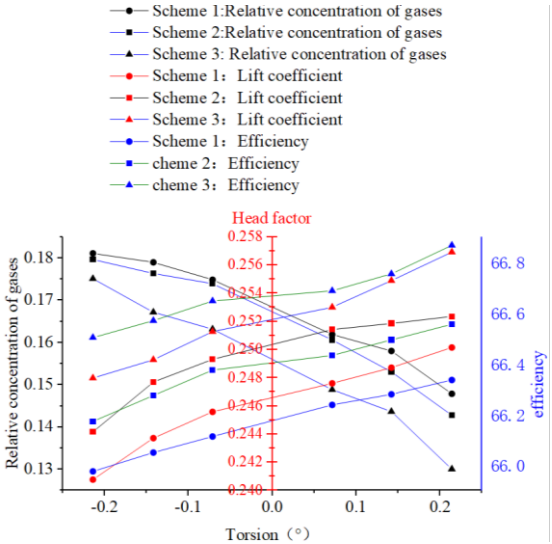

Fig. 18 Relative gas aggregation versus head coefficient and efficiency for schemes 1, 2 and 3

(i) Based on the relationship curve between the gas relative aggregation and degree of twist of the multiphase pump in Scheme 3, the results showed that the R_{vog} and the degree of twist were negatively correlated functions. The mathematical equation for R_{vog} with respect to the degree of twist τ was solved using a numerical fitting method.

The expression of the polynomial fitting curve is expressed as follows:

$$R=0.16-0.08\tau-0.09\tau^2-0.54\tau^3 \tag{13}$$

The larger the degree of twist, the smaller the relative gas aggregation. This indicates that the weaker the pressurization capacity of the impeller part of the mutiphase pump, the more remarkable the flow channel gas-phase aggregation and separation phenomenon, and the larger the energy loss.

(ii) Based on the relationship curve between the head coefficient and degree of twist of the mutiphase pump in Scheme 3, the mathematical equation of the head coefficient with respect to the degree of twist τ was solved using a numerical fitting method.

$$\psi=32.09+2\tau+1.05\tau^2+15.1\tau^3 \tag{14}$$

The head coefficient and degree of twist τ were positively correlated functions; that is, with an increase in the degree of twist, the pump head was improved to some extent. This indicated that the modification method had an improved effect on the head of the mutiphase pump.

(iii) The relationship curve between the efficiency and the degree of twist of the mutiphase pump shown in Scheme 3 indicates that the efficiency was positively correlated with the degree of twist.

$$\eta=66.66+0.38\tau+0.48\tau^2+10.5\tau^3 \tag{15}$$

The efficiency and degree of twist τ were positively correlated; with an increase in the degree of twist, the efficiency increased, and, at a degree of twist τ=0.214, the efficiency reached its maximum.

3.5.1 Effect of Twisted Vanes Based on Airfoil Twist on The Internal Flow Characteristics of the Multiphase Pump

The twisted airfoil cross-sections showed that changing the twist degree of the face4 resulted in an improvement in the gas-liquid two-phase flow on face4; thus, the degree of gas-phase aggregation in the flow channel was reduced.

As shown in Fig. 19, the twist degree of face 5 ranged from -0.214 to 0.214 from left to right. In this scheme, as the blade twists towards the suction side on the face4, the closer it gets to the trailing edge of the blade, the more severe the twist. When the twist degree was τ_1=-0.214, face4 experienced the most powerful deflection towards the suction side overall. As face 4 moved closer to the trailing edge on face4, the deflection became stronger. As the degree of twist τ_1 ranged from -0.214 to -0.0714, gas-phase aggregation became more severe, and the trailing-edge part of face 4 moved closer to the suction side,

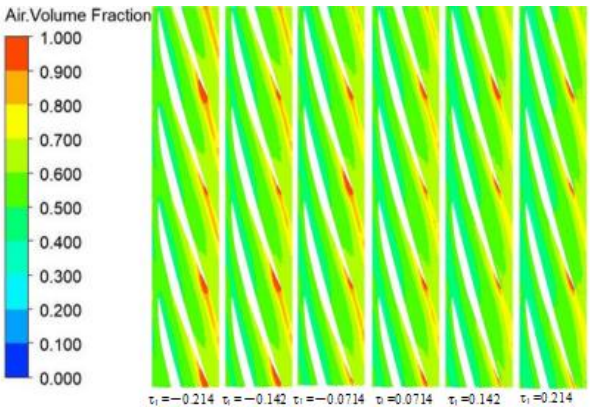

Fig. 19 Scheme 1 0.1 times the volume fraction of the gas at leaf height

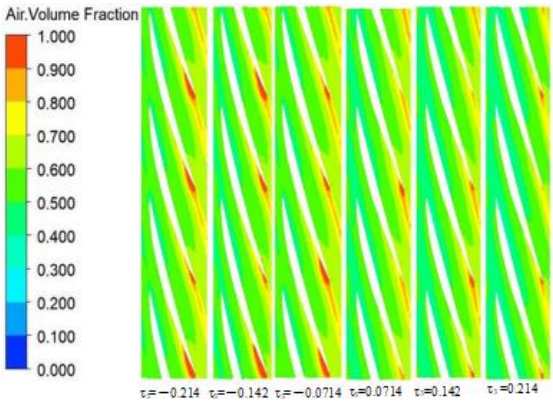

Fig. 21 Scheme 3 0.1 times the volume fraction of leaf height gas

intensifying the gas-phase aggregation. As |τ| increased, R_{vog} also increased, and the degree of gas aggregation increased in the latter half of the impeller runner. During the twisting process of the blade face4 towards the pressure side, the deflection became more powerful as it moved closer to the trailing edge of the blade. When the degree of twisting was τ_1=0.214, face 4 experienced the most powerful deflection towards the pressure side overall, with the deflection becoming stronger closer to the trailing-edge part in face4. As the degree of twist τ_1 ranged from 0.0714 to 0.214, R_{vog} was gradually relieved as face4 twisted towards the pressure side. The closer the trailing-edge part of face4 was to the pressure side, the more the degree of gas-phase aggregation was relieved. Moreover, as |τ| increased, R_{vog} decreased, and the degree of gas aggregation weakened in the latter half of the impeller runner. Therefore, Scheme 1 shows that twisting the face4 towards the pressure side for the same |τ| helps alleviate the gas aggregation phenomenon.

In Fig. 20, the degree of twist τ_2 is shown from -0.214 to 0.214 from left to right. During twisting in this scheme, the head and trailing edge of face4 were twisted in different directions. When twisted counterclockwise, the head of face4 twisted toward the suction side, while the trailing-edge part of face4 twisted toward the pressure side. The largest degree of face4 twisting counterclockwise occurred when τ_2=0.214. As |τ| increased, R_{vog} decreased,

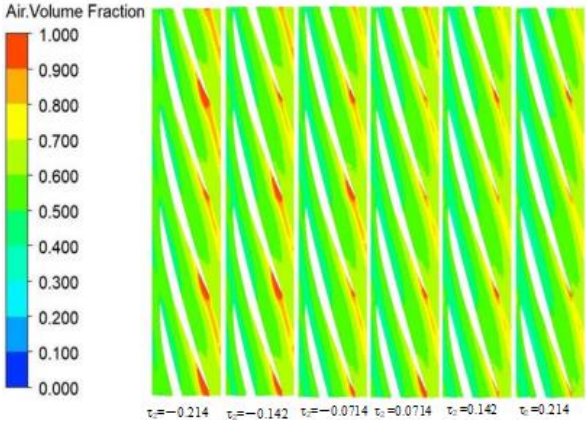

Fig. 20 Scheme 2 0.1 times the leaf height gas volume fraction

and the gas aggregation in the latter half of the impeller flow path weakened, resulting in a significant reduction and improvement in the degree of gas-phase aggregation. Clockwise twisting caused the head of face4 to twist toward the pressure side, and the trailing-edge part of the face4 to twist toward the suction side. When the degree of twist changed from τ_2=-0.0714 to τ_2=-0.214 in the process, the degree of gas-phase aggregation worsened at the trailing edge of the back side of the blade. As |τ| increased, R_{vog} increased, and this twisting worsened the degree of gas-phase aggregation. Overall, it can be concluded that twisting face4 counterclockwise in Scheme 2 helped to improve the gas aggregation phenomenon for the same |τ| case.

As shown in Fig. 21, the blade face4 was twisted towards the suction side in order of τ_3 from -0.214 to 0.214 from left to right. The degree of twist was stronger closer to the leading edge, and whenτ_3=0.214, the face4 was most twisted towards the suction side, with the head of the face4 being the most twisted. A degree of twist ranging from τ_3=0.0714 to τ_3=0.214 improved the degree of gas-phase aggregation and reduced the region with extra-high gas content. As |τ| increased, R_{vog} decreased, and the degree of gas-phase aggregation weakened in the latter half of the impeller flow path. Conversely, when the face4 twisted towards the pressure side, the twisting was stronger closer to the leading edge. When τ_3=-0.214, the twisting of the face4 towards the pressure side was most powerful, and a degree of twisting ranging from τ_3=-0.0714 to τ_3=-0.214 increased the degree of gas-phase aggregation. Increasing |τ| twisted the leading edge of the face4 towards the pressure side, which further aggravated gas-phase aggregation. As |τ| increased, R_{vog} increased, and the gas-phase aggregation phenomenon was aggravated in the latter half of the impeller flow path. Comparing cases with the same |τ| value, it was found that a greater offset towards the suction side in Scheme 3 alleviated the gas-liquid separation phenomenon.

3.5.2 Comparison of the Internal Flow Characteristics of Three Twisted Blade Schemes Based on Airfoil Twist

The cloud diagram in Scheme 3 showed the most remarkable improvement in the gas-liquid aggregation phenomenon. In Scheme 3, the twist degree τ_3 was 0.214,

face4 was twisted towards the suction side, the region with high gas content in the gas phase was significantly reduced, R_{vog} decreased, and the flow channel became smoother. This proves that, when |τ| is consistent, twisting the head of the face4 towards the suction side can more effectively slow down the gas-liquid separation phenomenon and reduce R_{vog}.

For Scheme 1, when face4 was twisted towards the pressure side with a larger |τ|, the twisting at the trailing edge of face4 was more severe, resulting the flow channel to be unobstructed. Conversely, when face4 was twisted towards the suction side with a larger |τ|, the twisting at the trailing edge of face4 was more severe, resulting in a more severe gas aggregation at the back of the blade. When |τ| was the largest, a flow vortex were also generated at the trailing edge of the blade.

For Scheme 2, when face 4 was twisted clockwise, an increase in |τ| aggravated the gas-gathering phenomenon in the flow channel, and caused mixture backflow. Conversely, when face4 was twisted counterclockwise, an increase in |τ| alleviated the gas aggregation phenomenon in the flow channel, resulting in a decrease in R_{vog}.

For Scheme 3, when face4 was twisted in the pressure direction with a larger |τ|, the twisting at the front edge of face4 towards the pressure side was offset. This generated a flow vortex. On the other hand, when face4 was twisted in the suction direction with a larger |τ|, the twisting at the head of face4 towards the suction side was increased, and R_{vog} decreased. This made it easier for the backflow phenomenon in the flow channel to disappear, enabling the channel to flow more smoothly.

4. CONCLUSION

In this study, a spiral axial-flow pump was used as the basic model. The influence of the formed twisting vane was explored based on airfoil twisting in the gas–liquid separation in a flow channel. Therefore, R_{vog} was proposed as a measure of the degree of gas-phase aggregation. Moreover, the bending and twisting vanes effectively improved the performance of the mutiphase pump, reduced the R_{vog} in the impeller part, and reduced the presence of a low-velocity zone at the trailing edge of the vane. The details are as follows:

(1) By studying the modification schemes of impeller blades, it was found that appropriate translation and twist of the airfoil near the hub of the blade can effectively reduce the relative gas accumulation in the second half of the impeller flow path, and have a certain effect on alleviating the backflow and gas stalling phenomena at the back of the blade.

(2) In the three schemes, the new face4 was formed by twisting with different twisting centers; in Scheme 3, the trailing-edge point of the face5 airfoil was taken as the twisting center. The twisted blade formed by twisting the head of face4 toward the suction side could effectively alleviate the gas aggregation phenomenon in the flow channel, reduce the R_{vog} in the back half of the impeller flow channel, and reduce the area of the low-velocity zone at the trailing edge of the back of the blade, thereby improving the gas flow blockage within the channel.

ACKNOWLEDGEMENTS

This study was funded by the National Natural Science Foundation of China [Grant No. 5217090851]; the National Key Research and Development Program Project [Grant No. 2018YFB0606100]; the Central Guidance for Local Science and Technology Development Fund Project (Development and Industrialization of Shallow Water Multiphase Flowmeter in Bohai Bay); the Key Technology Research for Renovation and Modification of Large-Scale Stepped Pump Station of Jingtai River Power Irrigation Project; and the Innovation Star Project of Gansu Province (2022CZZX-442).

CONFLICT OF INTEREST

No potential conflict of interest was reported by the authors.

AUTHORS CONTRIBUTION

Wei Han: Conceptualization; Funding acquisition; Supervision; Writing – original draft; Huimin Feng: Methodology, Project administration; Supervision; Writing – original draft; Writing – review & editing; Zitian Xu: Investigation; Writing – review & editing; Yingjian Hao: Writing – original draft; Investigation; Jing Zhang: Project administration; Chenkun Yang: Methodology; Writing – original draft.

REFERENCES

Deng, X., Yuan, S. Q., Si, Q. R., Yuan, J. P., & Zhang, J. F. (2014). Effects of twisted and cylindrical blades on the flow characteristics inside blade inlet and outlet for a centrifugal pump. *Applied Mechanics & Materials*, 494-495, 645-650. https://doi.org/10.4028/www.scientific.net/AMM.494-495.645

Kumar, A., & Saini, R. P. (2017). Performance analysis of a single stage modified Savonius hydrokinetic turbine having twisted blades. *Renewable Energy*, 113, 461-478. https://doi.org/10.1016/j.renene.2017.06.020

Li, Q., & Xue, D. (2000). Research on the development of oil and gas multi-phase mutiphase pump. *China Offshore Oil and Gas. Engineering*, 47-51+56-5+28. revised to 47-51,56. https://doi.org/10.3969/j.issn.1673-1506.2000.01.012

Liu, Z. (2005). *Study of the bending and twisting of the vane on the cavitation inhibition of axial flow pump.* Harbin Engineering University.

Lumsdaine, E., & Cherng, J. G. (1976). Influence of blade characteristics on axial flow compressor noise. *AIAA PAPER*, 76-570. https://doi.org/10.2514/6.1976-570

Lv, Y. Z., Jiang, D. X., & Jiang, Y. (2012). Numerical

simulation on small scale straight-blade and twisted-blade vertical axis wind turbine. *Advanced Materials Research*, 455-456, 334-338. https://doi.org/10.4028/www.scientific.net/AMR.455-456.334

Shi, H., Zou, W., Li, Y., & Huang, X. (2018). Effect of blade form on the internal flow field and pressure pulsation of series-parallel pumps. *China Rural Water Conservancy and Hydropower*, 189-195. https://doi.org/CNKI:SUN:ZNSD.0.2018-05-042

Di, L. H., He, X. J., & Lao X. S. (2012) Research status and development trend of oilfield multiphase flow pump. *General Machinery*, 68-71. https://doi.org/10.3969/j.issn.1671－7139.2012.10.035

Zhang, X., & Feng, J. (2015). Study on the hydraulic performance of twisted blade turbine. *Coal Mining Machinery*, 36(08), 121-123. https://doi.org/10.13436/j.mkjx.201508047

Zhang, Z., Cui, G., & Xu, C. (2005). *Turbulence theory and simulation*. Tsinghua University Press.

Zhu, Z., Wu, L., Tan, H., & Tang, Y. (2012). Experiment of cross-flow fan performance parameters and optimization of twist angle. *Mechanical Design and Manufacture*, 203-205. https://doi.org/10.3969/j.issn.1001-3997.2012.01.076